DOE/NASA/1022-78/30
NASA TM-78880

PERFORMANCE AND STABILITY ANALYSIS OF A PHOTOVOLTAIC POWER SYSTEM

Walter C. Merrill, Ronald J. Blaha, and Roy L. Pickrell
National Aeronautics and Space Administration
Lewis Research Center

August 1978

Prepared for
U.S. DEPARTMENT OF ENERGY
Office of Energy Technology
Division of Solar Energy

NOTICE

DOE/NASA/1022-78/30
NASA TM-78880

PERFORMANCE AND STABILITY ANALYSIS OF A PHOTOVOLTAIC POWER SYSTEM

Walter C. Merrill, Ronald J. Blaha,
and Roy L. Pickrell
National Aeronautics and Space Administration
Lewis Research Center
Cleveland, Ohio 44135

August 1978

Prepared for
U. S. Department of Energy
Office of Energy Technology
Division of Solar Energy
Washington, D. C. 20545
Under Interagency Agreement E(49-26)-1022

PERFORMANCE AND STABILITY ANALYSIS OF A PHOTOVOLTAIC POWER SYSTEM

by Walter C. Merrill, Ronald J. Blaha, and Roy L. Pickrell

Lewis Research Center

SUMMARY

Recently much emphasis has been placed on the conversion of solar energy to more useable energy forms. One method is the direct conversion of solar insolation to a dc voltage and current by the use of solar cells. This dc power can then be "inverted" to ac power compatible with commercial utility lines to drive various ac loads. This report studies the performance and stability characteristics of one such system, a 10 kVA photovoltaic power system. The system is studied using linear Bode analysis and a nonlinear analog simulation. Power conversion efficiencies, system stability, and system transient performance results are given for system operation at various levels of solar insolation. Additionally, system operation and the modeling of system components for the purpose of computer simulation are described in this report.

INTRODUCTION

Recently much emphasis has been placed on the conversion of solar energy to more useable energy forms. One method is the direct conversion of solar insolation to a dc voltage and current by the use of solar cells. This dc power can then be "inverted" to ac power compatible with commercial utility lines to drive various ac loads. This report studies the performance and stability characteristics of one such system, a 10 kVA photovoltaic power system.

The Terrestial Photovoltaic Project Office, as part of an DOE effort, is developing a 10 kVA Inverter/Controller subsystem for testing in a Photovoltaic Power System (PPS), at Lewis Research Center (LeRC). The purpose of the combined system (PPS) is to investigate the application potential of photovoltaic power sources to supplement and/or replace conventional energy supplies. The PPS is designed for operation in either of two modes, the stand alone mode (mode I) and the utility mode (mode II). Mode I requires a system load independent of other power generation sources. Power

injection in this mode is a function of load only. In mode II power from the PPS is injected into a commercial utility distribution system. The amount of power transferred in this mode will depend upon the solar array and its environmental conditions. Mode I operation is not considered in this report.

The PPS consists of five major blocks: (1) an array of solar cells, (2) the 10 kVA dc to ac power inverter, (3) the power system controller (PSC), (4) the pilot sensor array, and (5) the utility interface. The solar array directly converts solar insolation into dc power. The inverter transforms this dc power to 60 Hz ac power compatible with most electrically driven machines. The inverter design is an adaption, under LeRC contract, of an existing product line. Included in the inverter design is the inverter phase control, which adjusts the inverter output voltage phase to assure that the power injection into the utility line is at unity power factor (i.e., the output current is in phase with the utility line voltage). The PSC monitors system operation and adjusts array operating voltage (by setting the power level of the inverter) to achieve maximum power operation of the array. The power system controller (PSC) conceptual design was accomplished at LeRC. The detailed design, fabrication, and acceptance testing was accomplished under LeRC contract. The pilot sensor array provides the reference voltage from which the target operating voltage for the solar array is derived. The utility interface supplies a power sink, for absorbing the PPS output power without disturbing the utility voltage magnitude or phase (in operations and analysis the utility voltage is used as the reference phasor).

This report begins with a description of the major elements of the PPS. The report then describes an analysis of the stability and overall performance of the PPS. In particular, a linear stability analysis of the system at a high and low power operating condition is discussed. Additionally, a nonlinear analog simulation to more completely model component performance and system stability is presented. Finally, a discussion of the analysis results concludes this report.

PPS DESCRIPTION

For the subject simulation and analysis, the PPS is defined in block diagram form in figure 1. Dynamically, the important elements are (1) the solar array, (2) the power system controller, (3) the power inverter with its input and output filters (a 0.021 Farad capacitor and a 0.005 Henry choke, respectively), (4) the inverter phase controller, and (5) the reference utility line voltage. In this equivalent circuit, the pilot sensor array function is obtained from the solar array open circuit voltage data model. Figure 1 also indicates important system variables and the information/command flow in the system. A list of symbols is given in appendix A.

Energy conversion is accomplished by the solar array. Impinging direct solar

insolation is changed to a dc voltage and current. The power inverter converts dc power to ac power. The input filter capacitor isolates the array from the pulsating dc input current requirements of the inverter. The inverter output filter inductor suppresses the high frequency harmonics present in the synthesized 60 Hz output voltage. The PSC (in mode II) sets the operating voltage of the solar array by controlling the magnitude of the inverter output (generated) voltage. The inverter phase control maintains an inphase relationship between output line current and utility line voltage by adjusting the phase of inverter generated voltage. Each element is now discussed in more detail.

Solar Array

The solar array consists of several hundred interconnected solar cells. The current-voltage characteristics for each cell for different solar insolation levels and ambient temperatures are determined experimentally and are presented in figure 2. The entire array consists of 64 parallel connected strings of solar cells with 600 series connected cells per string. Therefore a total solar array characteristic could be obtained by a simple scaling of the individual cell characteristic as shown in figure 2. The ordinate intercept value of each curve is called the short circuit current and the abscissa intercept value the open-circuit voltage. A normalization of each curve by its open circuit voltage and short circuit current values yields a single curve representative of all temperature and insolation conditions (fig. 3). This representation is convenient for usage in a system simulation since only one nonlinear curve need be programmed.

The solar array characteristic of figures 2 and 3 can be approximated closely by a diode equation (ref. 1).

$$I_{SA} = I_{SA,N}\left\{1 - \exp\left[A\left(\frac{E_D}{E_{D,N}} - B\right)\right]\right\}$$

The constants were graphically determined for the data presented as $A = 10$ and $B = 1$. Solar array power is then

$$P_{SA} = E_D I_{SA} \tag{2}$$

The maximum power point is found from

$$\frac{\partial P_{SA}}{\partial E_D} = 0 \tag{3}$$

From (1), (2), and (3) the necessary optimality condition is

$$\frac{E_D}{E_{D,N}} = \frac{\exp\ 10(1 - E_D/E_{D,N}) \ - 1}{10} \tag{4}$$

This equation is satisfied when

$$E_D \approx 0.7823\ E_{D,N} \tag{5}$$

Thus, when operating in the presence of direct insolation, the array generates a dc power in accordance with the voltage-current characteristics of figure 2. Maximum power operation at all conditions can be approximated if the array output voltage is maintained at 0.80 times the open circuit voltage. In mode II operation this is one goal of the PSC.

Power System Control

The mode II configuration of the PSC is given in block diagram form in figure 4. The feedback voltage, E_D, is filtered by a three pole, 40 Hz, Butterworth filter to remove 120 Hz noise and compared to a reference voltage, E_{REF}. The voltage, E_{REF}, is selected proportional to E_{OC} such that

$$E_D = 0.8\ E_{OC}$$

when

$$E_{D,F} - E_{REF} = 0$$

The error signal is filtered by a 500 Hz, single pole, low pass filter to remove high frequency noise. The filtered error signal then drives a proportional-integral control to generate the inverter control voltage.

Power Inverter

The power inverter transforms dc input power generated by the solar array into single phase ac power compatible with most electrical machines. Conversion is

accomplished by approximating the sinusoidal inverter output voltage by a preprogrammed sequence of dc pulses. The resultant sequence is filtered to remove high order harmonics. Conceptually, the inverter can be considered an ideal power conversion device, that is, dc power in equals ac power out at every instant of time. Actual inverter losses can then be approximated by two resistances on the output side of the inverter. Figure 5 is a schematic of the filter capacitor, power inverter, and inverter output impedance. The resistance loss of the filter choke is negligible. Figure 6 is a phasor voltage diagram that approximates the dynamic magnitude and phase relationships of variables given in figure 5. Note that a steady state condition would be represented by a right triangle diagram where $\varphi = 0$. Also, phase is defined with respect to the utility line reference voltage.

Inverter control is accomplished by two means. First, E_{CONT} adjusts the magnitudes of the generated voltage and the line current. These magnitudes also are related by the inverter output impedance. The control variable, θ, sets the phase angle of the generated voltage to control the phase difference between line voltage and current. This phase angle is adjusted by the inverter phase control (IPC) circuit.

Inverter Phase Control

The inverter phase control, IPC, determines the phase difference between line voltage and line current by comparing square waves derived from these two signals. This difference serves as an error signal to a proportional-integral control. The control output drives a voltage controlled oscillator which can affect minor adjustments in the frequency of the generated voltage (ref. 2). These adjustments effectively set the generated phase, θ. The IPC, therefore, acts as a phase locked loop that sets inverter generated phase such that $\varphi = 0$ in steady state. This inphase line voltage-line current condition insures maximum power injection by the inverter into the utility power line.

LINEAR ANALYSIS

In the initial phase of the investigations, a linear analysis was undertaken to investigate the stability of the PPS. This analysis was required to verify basic stability of the total system since individual components were being manufactured at different locations. Several assumptions were made to simplify this "first look" analysis. First, the system was linearized at both a maximum and minimum power operating condition to obtain Laplace transfer functions for each of the blocks in figure 7. Second, the inverter was assumed to be in a phase-locked mode at all times so that only the power control loop was active. Standard Bode analysis (ref. 3) was performed

using the transfer functions of appendix B. The dynamic resistance of the solar array, R_{SA}, is defined as the negative reciprocal of the slope of the solar array characteristic at the point of maximum power. For a high and low level of insolation two values of R_{SA} were used.

$$R_{SA}(\text{high}) = 4$$

$$R_{SA}(\text{low}) = 200$$

The results of the Bode analysis, given in figures 8 and 9 demonstrate that the nominal or high insolation condition is only marginal stable. A stability condition exists when at 180^{o} phase shift the open loop gain is less than 1. At the low insolation condition the system is unstable by a gain margin of 8.5 dB (gain factor of 2.7). A reduction in closed loop static gain of 12 dB will stabilize the system at both operating conditions leaving adequate stability margin at the low insolation condition. Thus, the PPS configuration with the reduction in loop gain can be expected to operate in a stable manner over a wide range of insolation levels. Further analysis of the impact of system nonlinearities and the IPC on system performance and stability was desired. To complete this analysis a nonlinear, analog simulation of the PPS was devised.

NONLINEAR ANALYSIS

The nonlinear analysis of the PPS further evaluated the stability of the system to varying solar insolation conditions. Also, transient system performance and tolerance to line voltage disturbances were studied. This section describes the nonlinear simulation and then discusses simulation test results.

Nonlinear Simulation

The nonlinear simulation was devised by combining component models to simulate the information flow of figure 1. Equations for each component are given in appendix C. The normalized solar array characteristic was approximated by 15 straight line segments to simulate solar array operation. Four characteristics generated by the analog simulation from the normalized curve by appropriate scaling are presented in figure 10 for comparison with the given characteristics of figure 2. Modeling equations for the PSC and the filter capacitor were determined from their circuit diagrams in a straightforward manner. Conceptually, the inverter was modeled as in reference 4. Equations and parameter values for the inverter and inverter phase controller components were obtained from the inverter manufacturer. Equations that model or

approximate the dynamic operation of the inverter output filter impedance were determined from trigonometric relationships associated with the phasor diagram of figure 6.

Equations (C3) to (C5) are a macroscopic or input-output representation of inverter operation. Considerable detail about internal inverter operation, such as the actual dc to ac voltage inversion and control processes was eliminated to simplify the simulation. Also, some approximations were incorporated such as considering the phase of E_1 and E_A to be identical. Digital computer simulation of the exact trigonometric equations at several operating points showed the approximation error to be negligible. In equation (C14) the approximations

$$\varphi \cong \sin \varphi$$

$$\theta \cong \sin \theta$$

are used. Equation (C14) should be written with φ and θ as dependent and independent variables, respectively. However, since φ and θ are generally less in magnitude than 0.7854 radians (45°), and since $\sin \theta$ and not θ is available from the simulation, the approximation of (C14) was used.

Another simplifying approximation is the phasor triangle representation of figure 6 for inverter output impedance. This is a more important limitation since it limits the maximum useful simulation bandwidth. The voltages and currents in the impedance network are usually sinusoidal in nature. In this case the phasor representation of figure 6 is well defined and accurately models the process. However, transient results for time intervals less than one period (0.0159 sec) of the phasor frequency (60 Hz) and disturbances that generate a nonsinusoidal inverter output voltage are not accurately represented. These modes of operation can occur for brief intervals during line transients. Because of their brief duration and because the simulation accurately models the trends for these brief intervals, this limitation does not seriously impact the usefulness of the simulation.

Experimental Results

Several experiments completed with the nonlinear simulation were used to evaluate system (1) stability, (2) transient performance, and (3) steady-state efficiencies.

Stability

The linear analysis indicated that instability, if it were to occur, would be most likely at low insolation levels. Thus, to determine the critical insolation level at which instability occurs, as well as simulating system operation during a worst case "cloud cover" transient, the following experiment was devised. Insolation level was

decreased at constant rate from 100 to 6.5 mW/cm^2 in 5 seconds, held at 6.5 mW/cm^2 for approximately 6 seconds, then increased at constant rate to 100 mW/cm^2 in 5 seconds. The experiment was conducted using the nonlinear simulation with a constant line voltage magnitude, $E_{L,M} = 340$ volts, and a constant reference point setting of $E_D = 0.8\ E_{OC}$. The PSC forward gain was nominally selected as $K = 5$. This setting corresponds to the reduced stabilizing gain found in the linear analysis. Insolation level changes were simulated by varying the normalizing values for the solar array characteristic according to (C19).

Time records of the cloud cover transient are given in figure 11 for several system variables. For the cloud cover transient ambient solar cell temperature was assumed to be 55^o C. Overall, system operation is stable for almost the entire transient, that is, a nonoscillatory, smooth trajectory for the solar array operating point is achieved. However, a limit cycle is observed in the inverter phase control portion of the system for insolation levels less than 20 mW/cm^2. Additionally, the solar array voltage, E_D, oscillates about its commanded value. This loss of control and subsequent inverter phase control oscillation is a result of the small difference in magnitude between generated and line voltages. From figure 11 the onset of the limit cycle occurs when $E_{A,M}$ (or $E_{1,M}$) appears equal to $E_{L,M}$. From figures 5 and 6 $E_{1,M}$ always must be greater than $E_{L,M}$ in steady state. From table I at 20 mW/cm^2, $E_{1,M} - E_{L,M} = 0.72$ volts. This is a difference of only 0.18 percent. Practically, the analog computer used to implement the nonlinear simulation cannot resolve this difference. Conceptually, this can be modeled as a deadzone nonlinearity in the system. Therefore, ability to set θ and injected power is lost, a power imbalance is incurred, and localized limit cycling results. Similar results may be anticipated from the actual system since it will be equally difficult for any real hardware to maintain accurate power level control by resolving such small voltage differences.

Transient Performance

The transient response of the PPS to changes in the commanded reference point and to changes in the utility line voltage were also simulated. Responses to reference point step changes define dynamic response times of the system. System response to utility line voltage fluctuations is particularly important since this is typically the most severe operating constraint on utility mode operation.

Figures 12 to 15 show system response to ±10 percent changes in E_{REF} for four insolation levels, 100, 33, 14, and 6.5 mW/cm^2, respectively. These experiments were conducted with $E_{L,M} = 340$ volts and $K = 5$. As E_D changes the PSC and the inverter must adjust the generated voltage, line current, etc. to satisfy the change in

available solar power. Since $E_{L,M}$ is constant, $I_{L,M}$ must change in direct proportion to available power. From (C4) E_{CONT} and $I_{L,M}$ are directly related in steady state. In each case the overall dynamic response, reflected chiefly in E_{CONT}, is the same. At the two low insolation level conditions the IPC cycling is evident. Although precise voltage control and power injection is not being accomplished in these two cases, global system stability is maintained in the presence of the operating point disturbances. In the 100 and 33 mW/cm^2 cases adequate set point control is accomplished. System response is basically characterized as underdamped and second order. More damping, if desired, could be obtained by reducing PSC forward gain.

Figures 16 to 19 show system response to ±10 percent changes in the magnitude of line voltage. These changes represent worst case line voltage transients that the PPS must tolerate. These experiments were also conducted at 100, 33, 14, and 6.5 mW/cm^2. Nominally, $E_{L,M} = 340$ volts and $K = 5$. As $E_{L,M}$ step changes are encountered, the IPC adjusts θ and the PSC adjusts E_{CONT} to match the new level of line current. For the 100 and 33 mW/cm^2 experiments line transient tolerance is good. Notice that as insolation level decreases the line transients have a more pronounced effect on system operation. This is true since the 10 percent line voltage transient causes a higher percentage power imbalance at lower insolation levels. Again at the 14 and 6.5 mW/cm^2 levels, global system stability is maintained for these line transients although accurate voltage and power control is lost.

Efficiency

This performance test was conducted to predict operating efficiencies and power levels at various solar insolation levels. Steady-state data were recorded and are listed in table I. System efficiency is calculated as

$$\eta = \frac{E_{L,M} I_{L,M}}{2E_D I_{SA}} = \frac{P_L}{P_{SA}}$$

A comparison of simulation and design inverter efficiencies is given in figure 20. The values of the two power loss resistors in the inverter output impedance were selected to match the simulation to the design efficiencies at two power level points, no load and rated power. Resistor RL1 represents resistive or load losses while RL2 represents no load power required for inverter operation. Figure 20 shows a good correspondence throughout the operating range. A comparison of the design and simulated power loss, as in figure 21, shows an essentially constant difference in power loss which the model does not account for. This loss discrepancy was not investigated in depth. However,

it was noted that in the inverter power switching transistors the diode junction losses are a linear function of load current rather than a squared function as indicated by the resistive element. Improved performance correlation could be obtained if necessary, by incorporating this source of power loss differently in the simulation.

SUMMARY OF RESULTS

A preliminary analysis of stability of the PPS demonstrated possible instability for the specified design value of PSC forward gain. From the linear analysis a gain reduction of 12 dB was found sufficient to stabilize the system at the high and low insolation levels studied. Subsequent nonlinear simulation confirmed global system stability over the entire range of insolation levels with the reduced PSC forward gain. However, a limit cycle was encountered in the IPC subsystem for insolation levels less than 20 mW/cm^2. This limit cycle phenomenon was found to be the result of a deadzone effect. The actual PPS will probably exhibit this limit cycle since the deadzone is encountered for small differences in line and inverter output voltage which naturally result from low insolation levels.

For insolation levels above 20 mW/cm^2 the system exhibited (1) good operating point control of the desired solar array voltage and accurate control of utility line power injection for the cloud cover transient, (2) an underdamped, second order response to E_{REF} transients, and (3) acceptable rejection of ±10 percent line voltage step transients. For insolation levels below 20 mW/cm^2 acceptable system stability and solar operating voltages were maintained for all the above experiments. However, oscillations in injected utility line power and solar array voltage were encountered.

APPENDIX A

SYMBOLS

D( )	derivative operator, sec^{-1}
E	voltage, V
exp	Naperian exponential
F1 to F5	PPS transfer functions
f1	normalized array characteristic
I	current, A
j	$\sqrt{-1}$
K	PSC forward loop gain
L	filter choke inductance, Henry
R	effective resistance, ohm
RL1	inverter loss resistance, ohm
RL2	inverter loss resistance, ohm
s	Laplace variable, sec^{-1}
η	system efficiency
θ	inverter output voltage phase angle, rad
φ	line current phase angle, rad
Subscripts:	
A	ideal inverter output (AC)
CONT	PSC
D	inverter input (DC)
F	filtered
L	line
M	magnitude
N	normalized
OC	open circuit
REF	solar array operating point

SA	solar array
SC	short circuit
X	filter choke reactive component
1	actual inverter output (AC)

APPENDIX B

PPS TRANSFER FUNCTIONS

$$F1(s) = \frac{20}{0.000318\ s + 1} \tag{B1}$$

$$F2(s) = \frac{s + 1}{s} \tag{B2}$$

$$F3(s) = \frac{10}{0.159\ s + 1} \tag{B3}$$

$$F4(s) = \frac{0.0156}{(0.00794\ s+1)\left[\left(\frac{s}{126}\right)^2 + \left(\frac{s}{126}\right) + 1\right]} \tag{B4}$$

$$F5(s) = \frac{R_{SA}}{0.021\ R_{SA} s + 1} \tag{B5}$$

APPENDIX C

NONLINEAR SIMULATION EQUATIONS

Solar array:

$$\frac{I_{SA}}{I_{SA,N}} = f_1\left(\frac{E_D}{E_{D,N}}\right) \tag{C1}$$

Filter capacitor:

$$D(E_D) = \frac{I_{SA} - I_D}{0.021} \tag{C2}$$

Power inverter:

$$E_D I_D = \frac{E_{A,M} I_{A,M}}{2} \cos(\theta - \varphi) \tag{C3}$$

$$D\left(\frac{E_{A,M}}{E_D}\right) = 4.358(E_{CONT,F} - 0.0664\, I_{L,M} \cos \varphi) \tag{C4}$$

$$D(E_{CONT,F}) = \frac{E_{CONT} - E_{CONT,F}}{0.159} \tag{C5}$$

Inverter output impedance:

$$\sin \varphi = \frac{E_{L,M}^2 + E_{X,M}^2 - E_{1,M}^2}{2E_{L,M}E_{X,M}} \tag{C6}$$

$$E_{X,M}^2 = E_{L,M}^2 + E_{1,M}^2 - 2E_{L,M}E_{1,M} \cos \theta \tag{C7}$$

$$I_{L,M} = \frac{E_{X,M}}{1.885} \tag{C8}$$

$$\cos \theta = \sqrt{1 - \sin^2 \theta} \tag{C9}$$

$$\cos \varphi = \text{sgn}(\sin \theta)\sqrt{1 - \sin^2 \varphi} \tag{C10}$$

$$E_{1,M} = E_{A,M} - 0.33\, I_{L,M} \tag{C11}$$

$$I_{A,M} = I_{L,M} + \frac{E_{1,M}}{300} \tag{C12}$$

$$\cos(\theta - \varphi) = \cos \theta \cos \varphi + \sin \theta \sin \varphi \tag{C13}$$

Inverter phase control:

$$(D^3 + 12.22\, D^2 + 27.97\, D)(\sin \theta) = -27.97(0.4368\, D + 1)(\sin \varphi) \tag{C14}$$

Power system control:

$$(0.00794\, D + 1)\left[\left(\frac{D}{126}\right)^2 + \left(\frac{D}{126}\right) + 1\right](E_{D,F}) = 0.0156\, E_D \tag{C15}$$

$$D\left[0.318(10^{-3})D + 1\right](E_{CONT}) = K(D + 1)(E_{D,F} - E_{REF}) \tag{C16}$$

$$E_{REF} = 0.0125\, E_{OC} \tag{C17}$$

$$E_{D,N} = E_{OC} \tag{C18}$$

$$I_{SA,N} = 0.662\, E_{D,N} - 164.05 \tag{C19}$$

REFERENCES

1. Angrist, S. W.: Direct Energy Conversion. Allyn and Bacon, Inc., Boston, 1965.

2. Nash, Garth: Phase-Locked Loop Design Fundamentals. AN-535, Motorola Semiconductor Products, Inc., 1970.

3. Dorf, R. C.: Modern Control Systems. Addison-Wesley, 1967, pp. 177-200.

4. Middlebrook, R. D.; and ´Cuk, Slobodan: Modeling and Analysis Methods for DC to DC Converters. IEEE International Semiconductor Power Conversion Conference, 1977, pp. 90-111.

5. O'Sullivan, G.: Technical Progress Narrative Report No. 01-Contract NAS3-20607, Abacus Controls, Inc.

TABLE I. - SIMULATION PERFORMANCE DATA

Variable	Insolation level, mW/cm^2					
	65	20	38	75	100	110
	Ambient temperature, ^{o}C					
	55	55	55	55	55	0
E_{OC}, V	252	266	285	292	310	375
I_{SC}, A	2.84	12.0	16.3	32.0	41.2	46.4
E_D, V	202	213	228	234	248	301
I_{SA}, A	2.38	10.4	13.7	26.8	34.6	38.9
$E_{L,M}$, V	340	340	340	340	340	340
$I_{L,M}$, A	1.69	11.7	16.9	34.5	47.1	63.8
$Power_{SA}$, kW	0.481	2.22	3.12	6.27	8.58	11.71
$Power_L$, kW	0.287	1.99	2.88	5.87	8.01	10.85
η	0.596	0.90	0.921	0.936	0.933	0.926
θ, deg	0.536	3.72	5.35	10.82	14.6	19.4
E_{AM}, V	340.96	345.01	347.50	357.85	366.95	380.93
E_{IM}, V	340.01	340.72	341.49	346.15	351.35	360.45
$I_{A,M}$, A	2.82	12.87	18.04	35.60	48.12	64.63
E_{CONT}, V	0.1120	0.7791	1.123	2.289	3.120	4.216

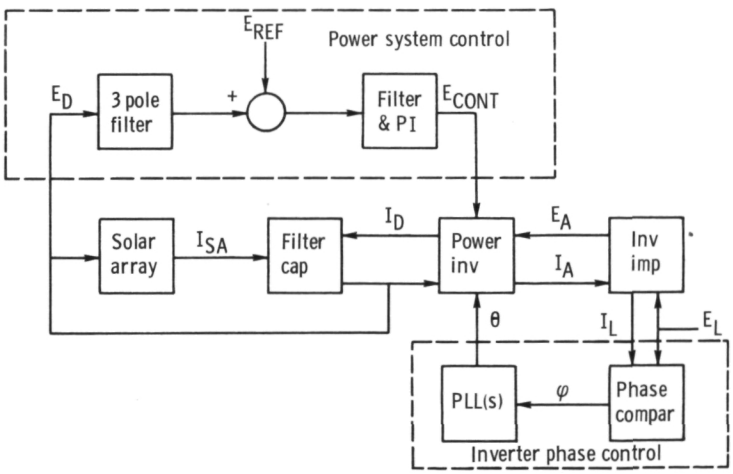

Figure 1. - Photovoltaic power system information flow diagram.

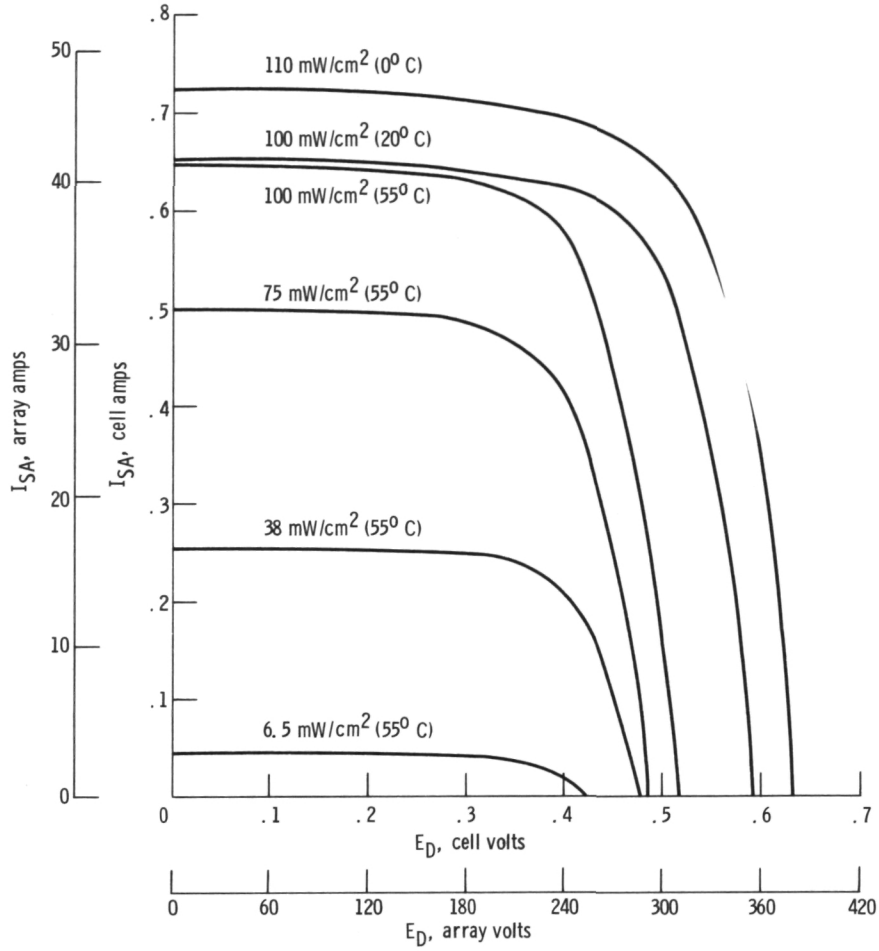

Figure 2. - Solar cell and solar array voltage-current characteristics.

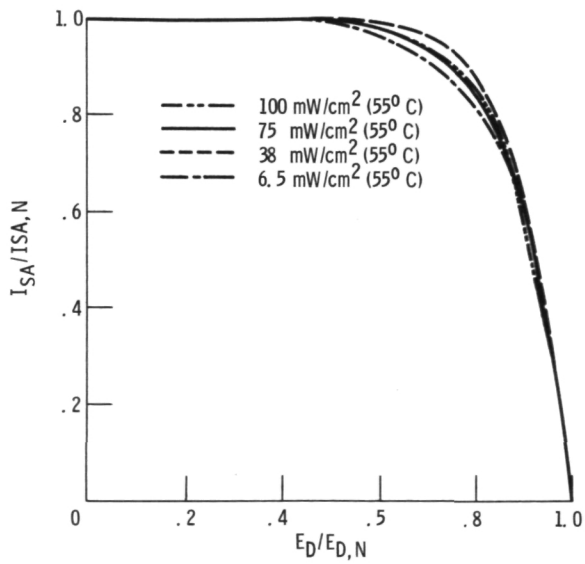

Figure 3. - Normalized solar array characteristic.

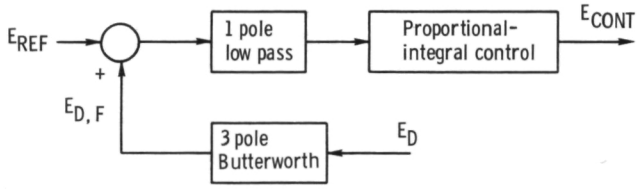

Figure 4. - Power system control block diagram.

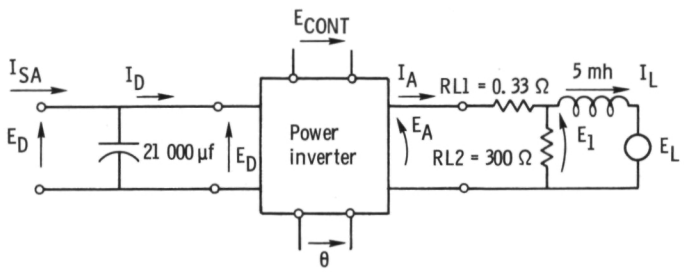

Figure 5. - Inverter schematic.

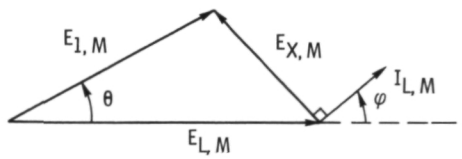

Figure 6. - Inverter output impedance voltage triangle.

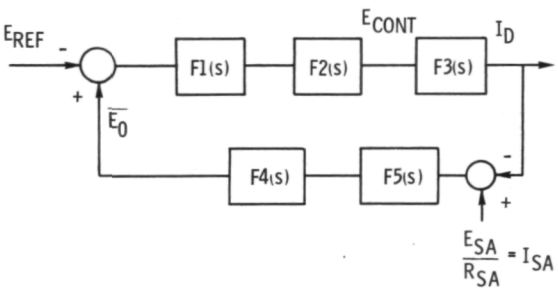

Figure 7. - Photovoltaic power system linearized block diagram.

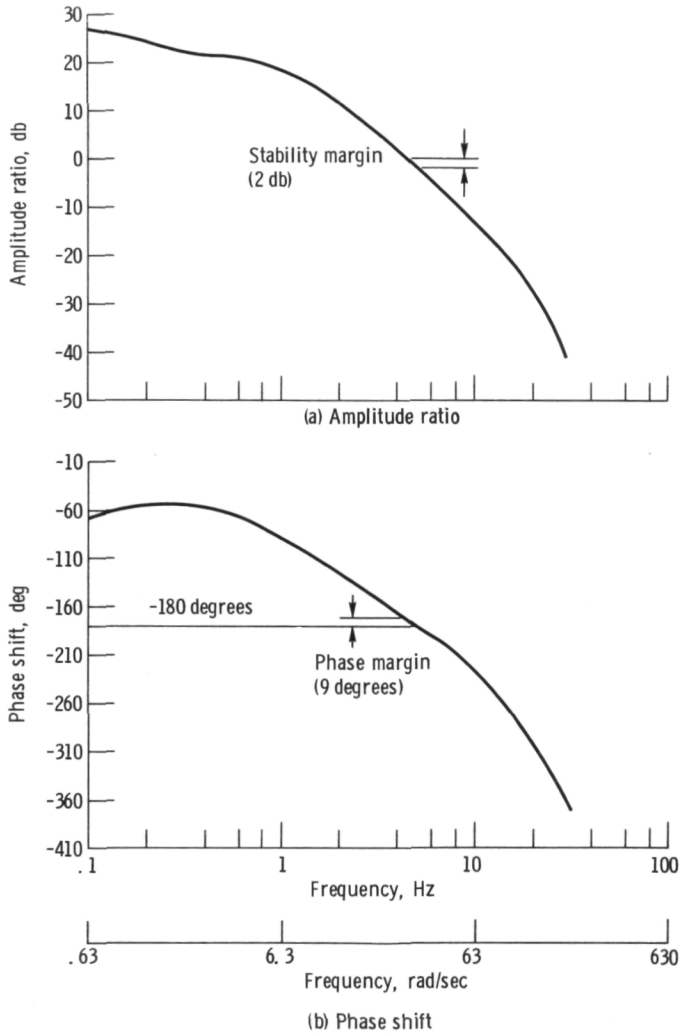

Figure 8. - Open loop frequency response of the linearized photovoltaic power system with $R_{SA} = 4$.

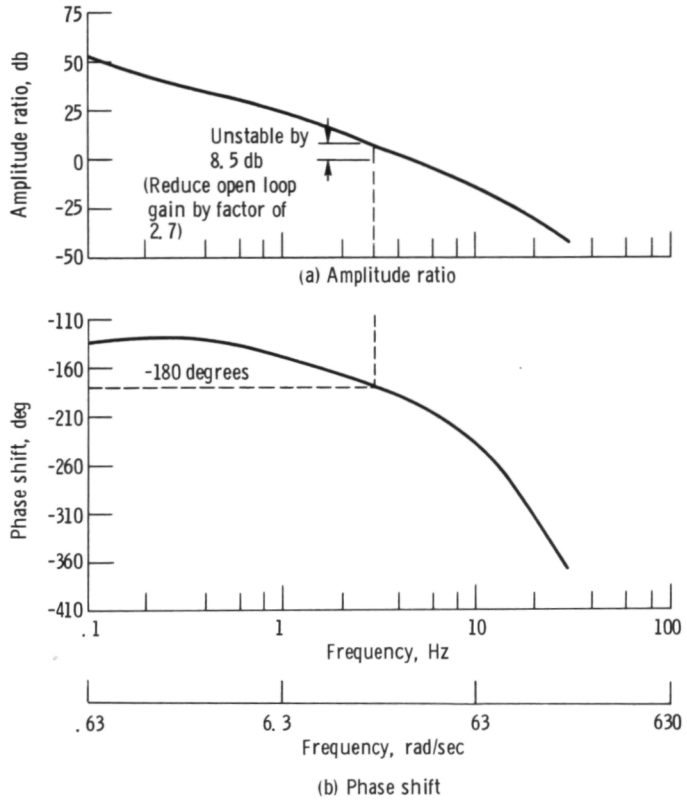

Figure 9. - Open loop frequency response of the linearized photovoltaic power system with R_{SA} = 200.

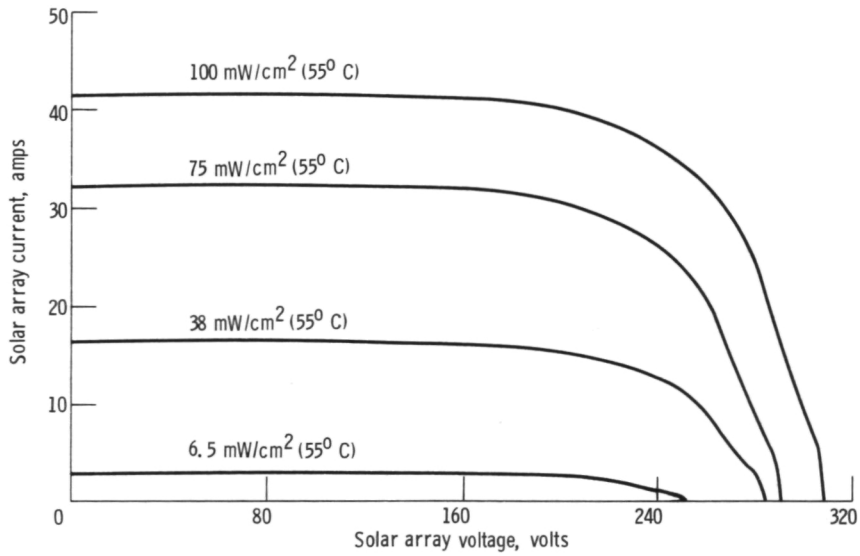

Figure 10. - Simulated solar array characteristics.

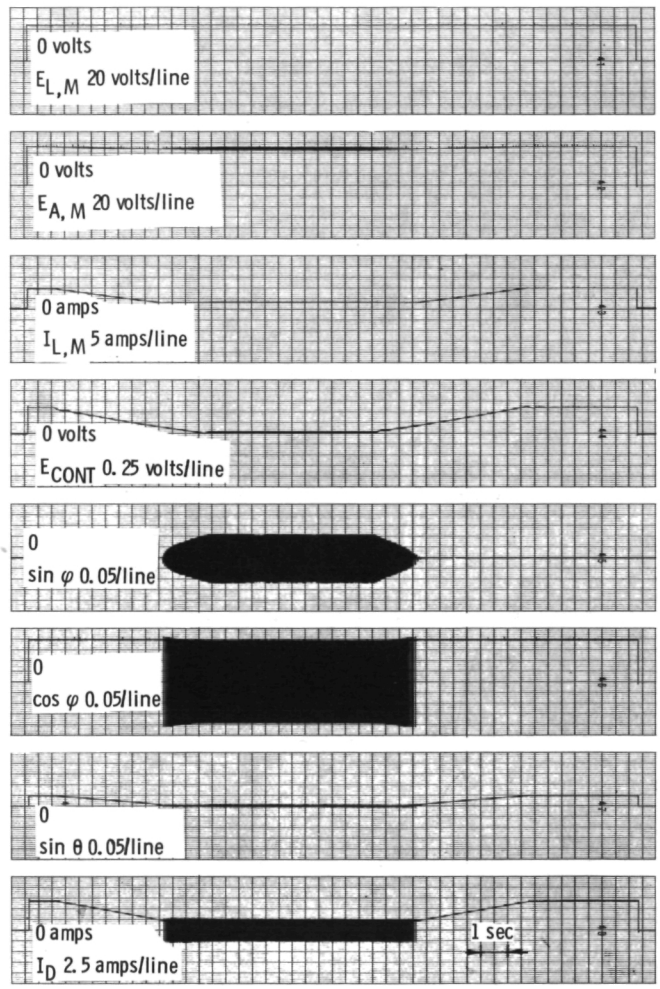

Figure 11. - Cloud cover transient from 100 mW/cm^2 to 6.5 mW/cm^2.

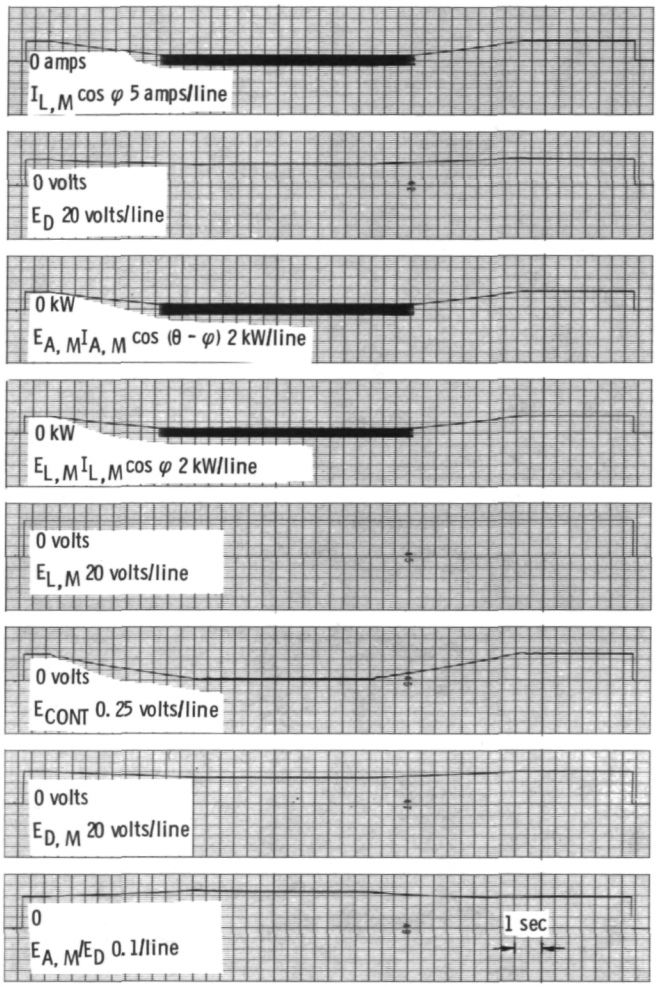

Figure 11. - Concluded.

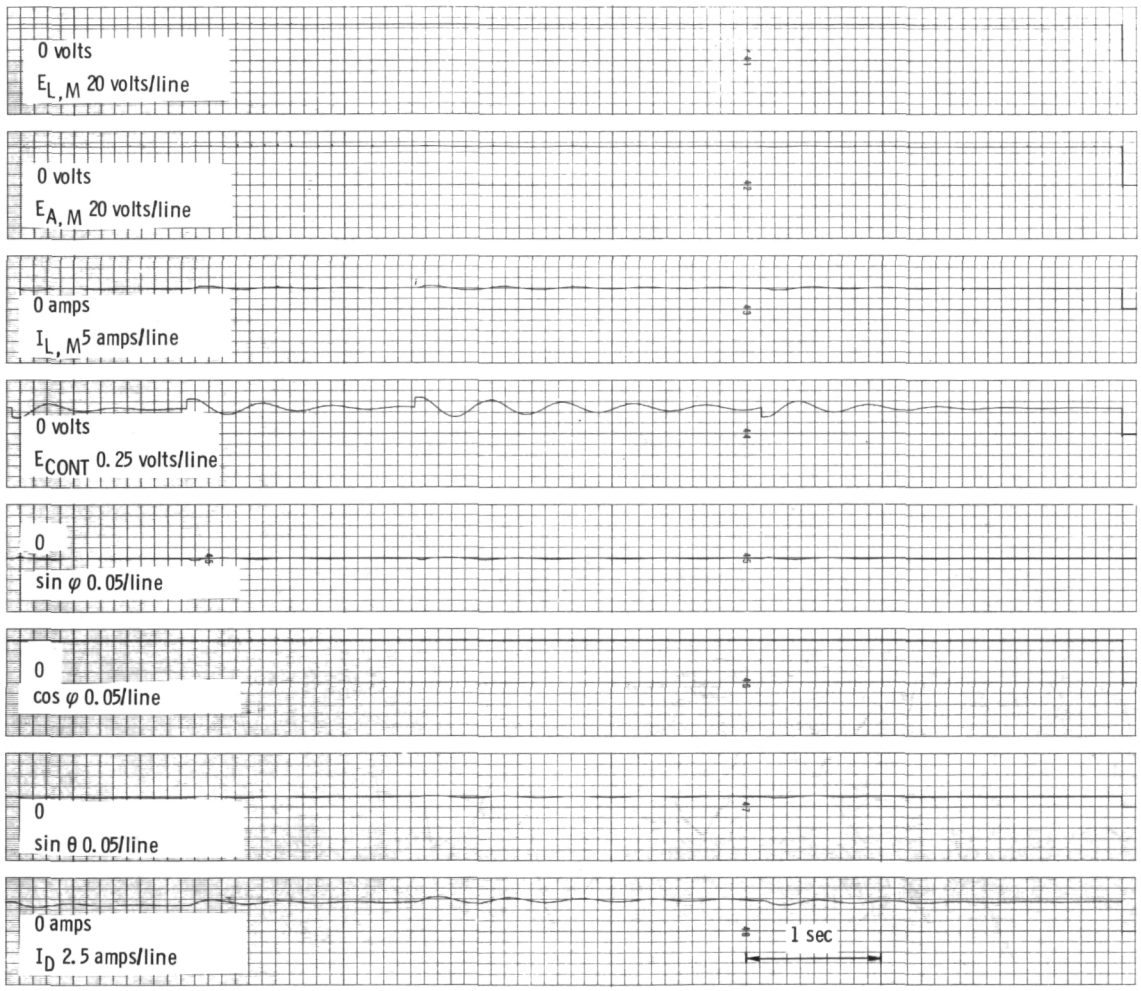

Figure 12. - ±10% step transients on E_{REF} at 100 mW/cm^2.

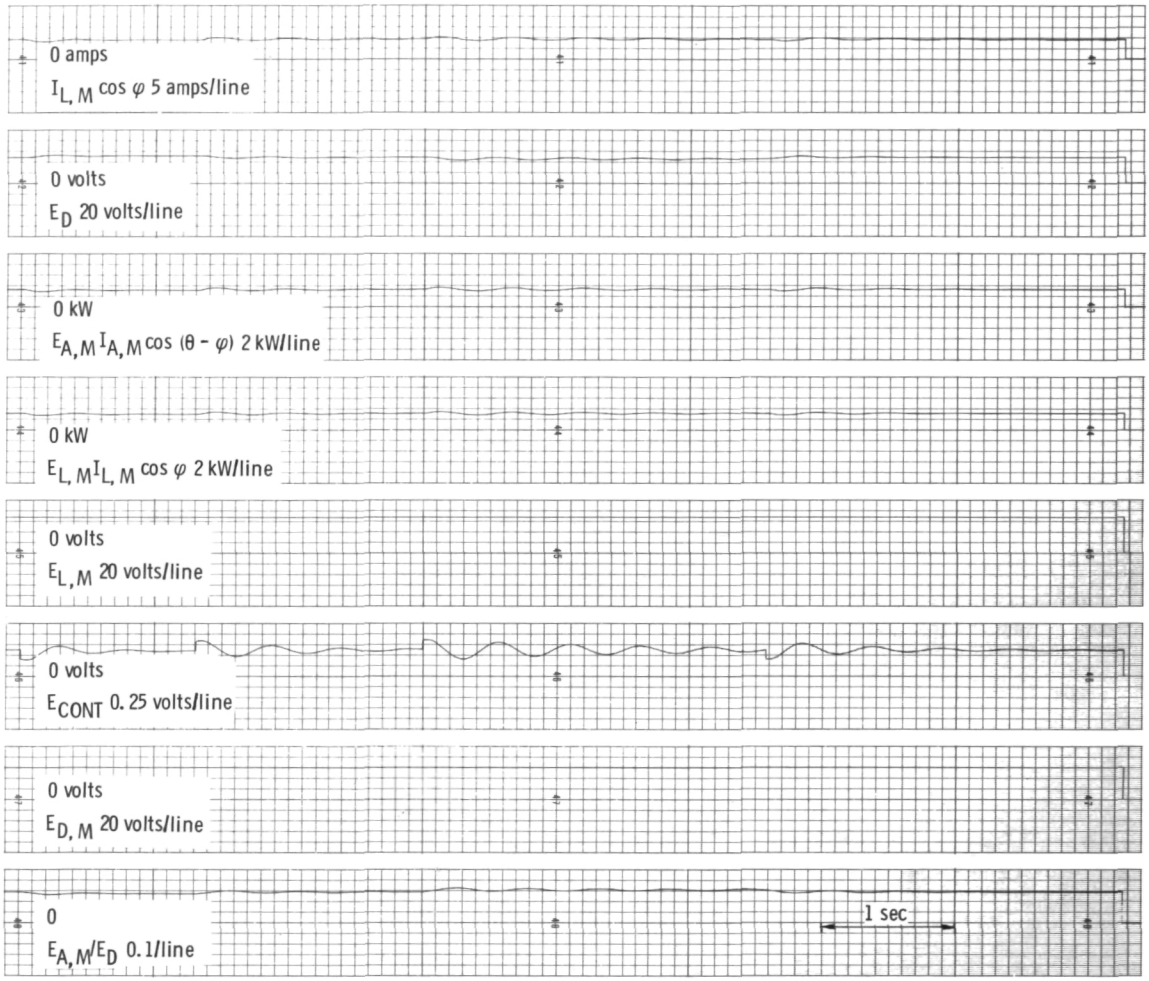

Figure 12. - Concluded.

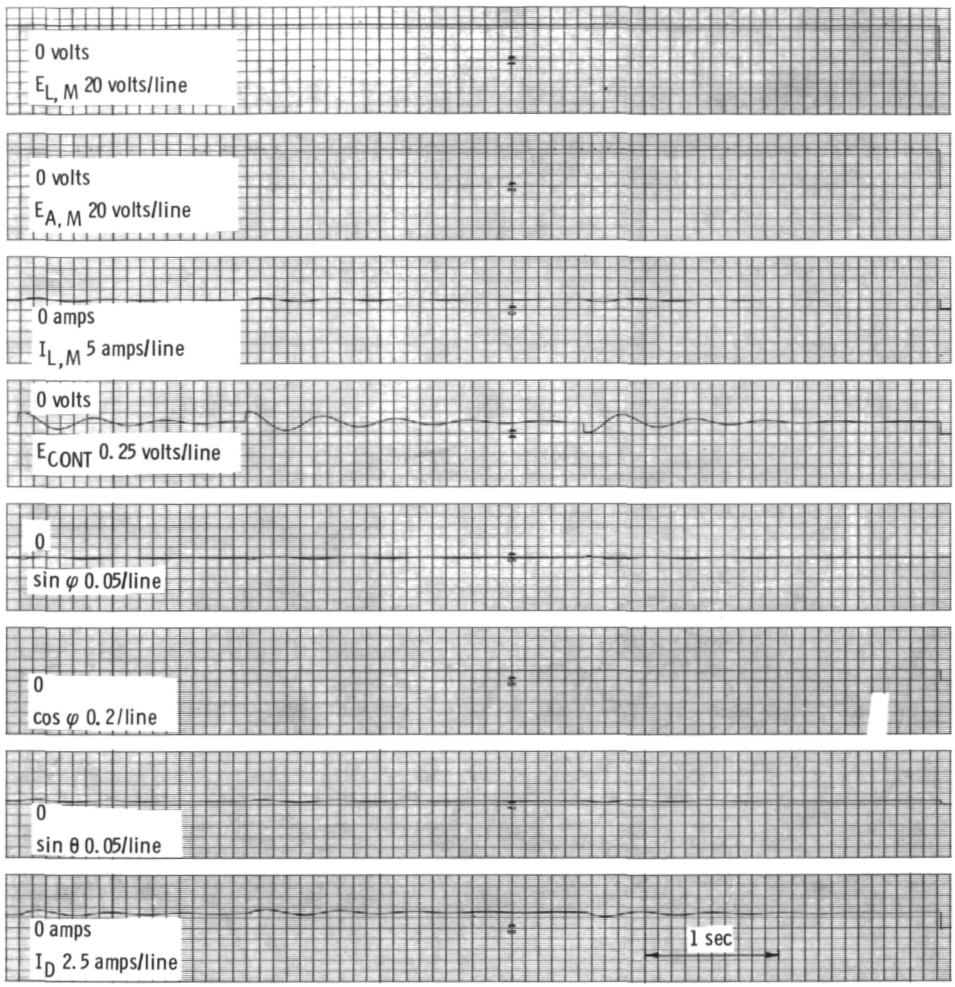

Figure 13. - ±10% step transients on E_{REF} at 33 mW/cm^2.

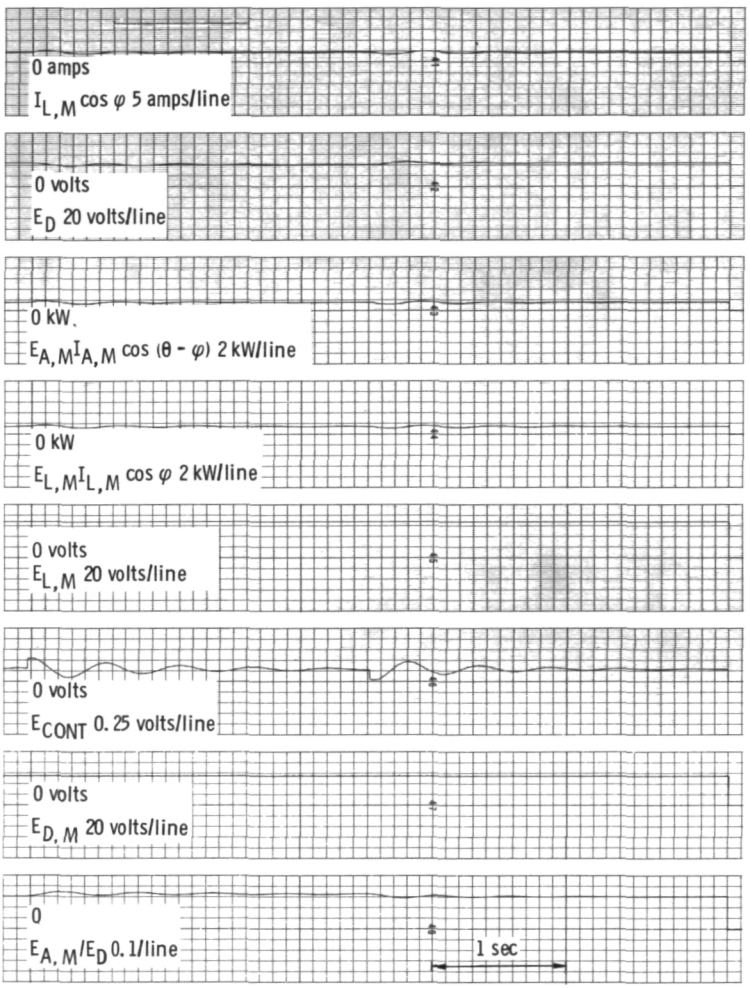

Figure 13. - Concluded.

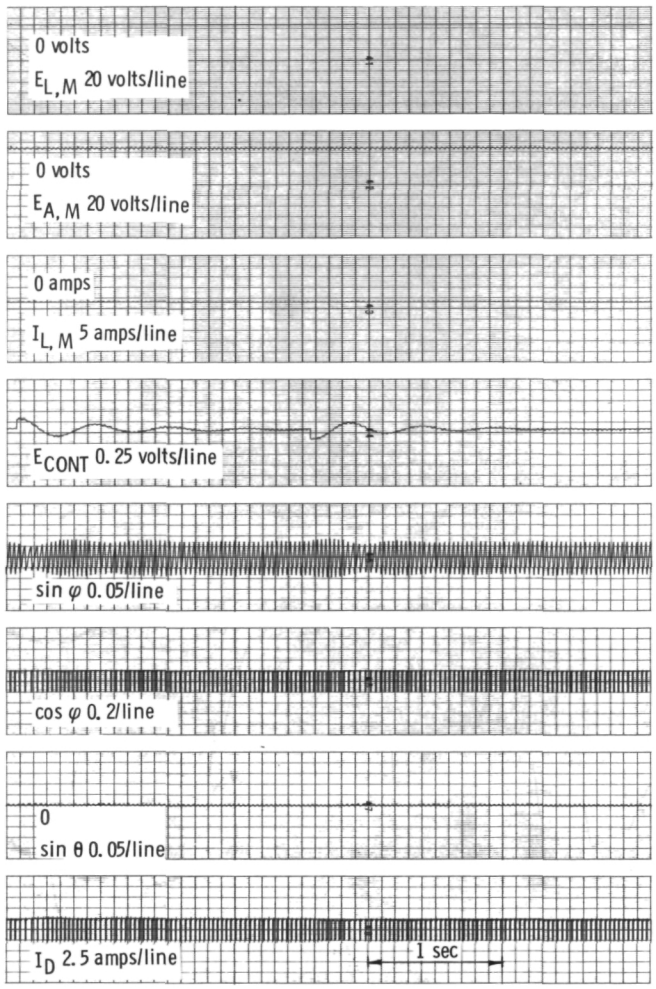

Figure 14. - ±10% step transients on E_{REF} at 14 mW/cm^2.

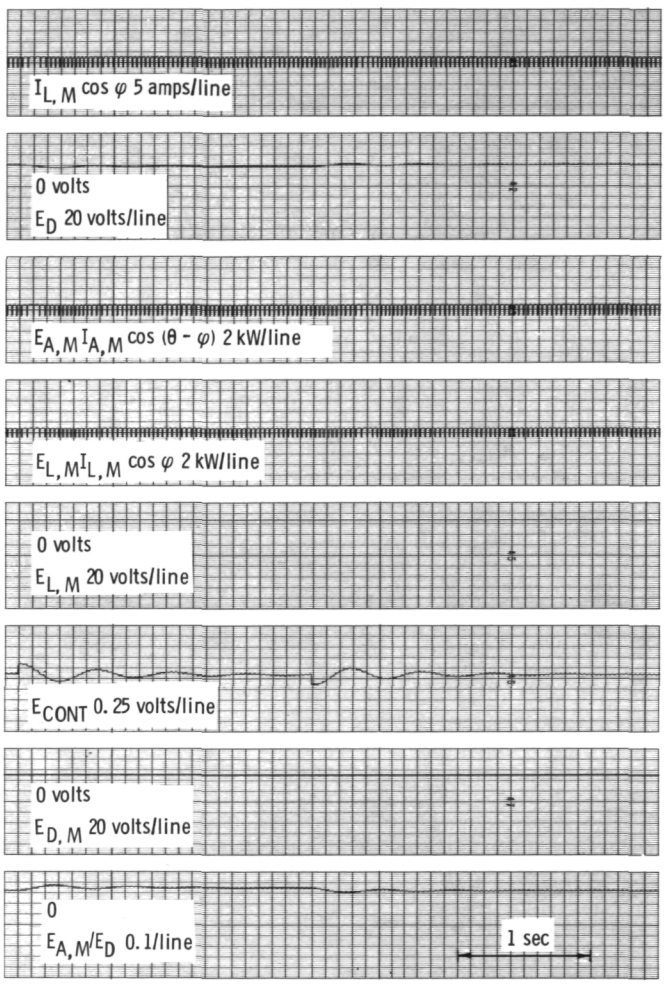

Figure 14. - Concluded.

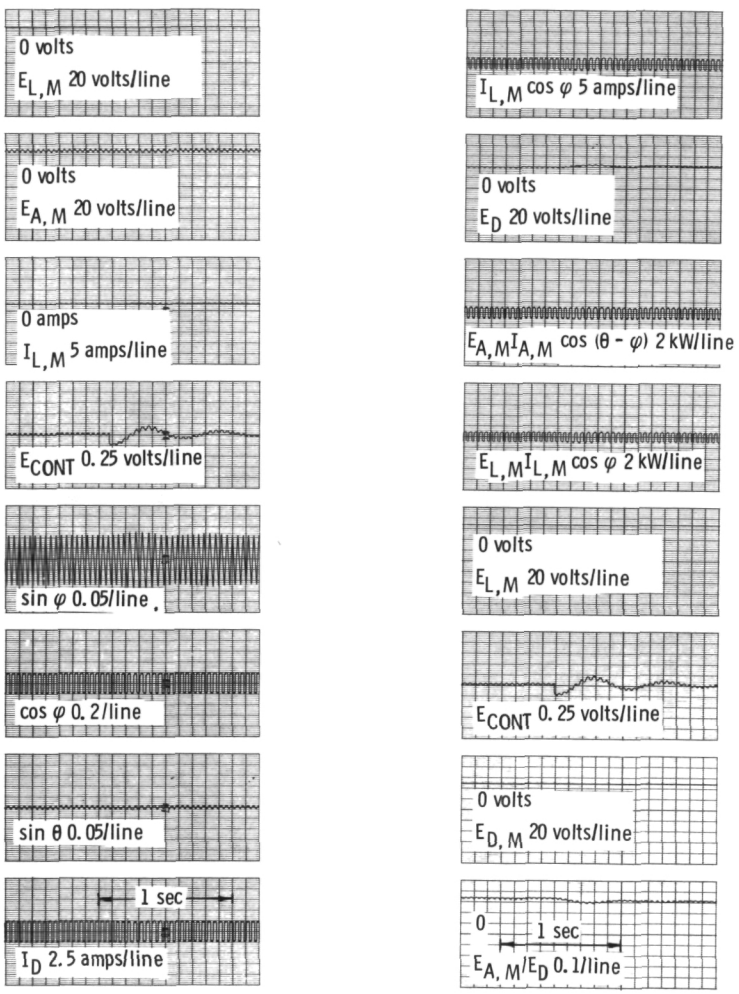

Figure 15. - ±10% step transients on E_{REF} at 6.5 mW/cm^2.

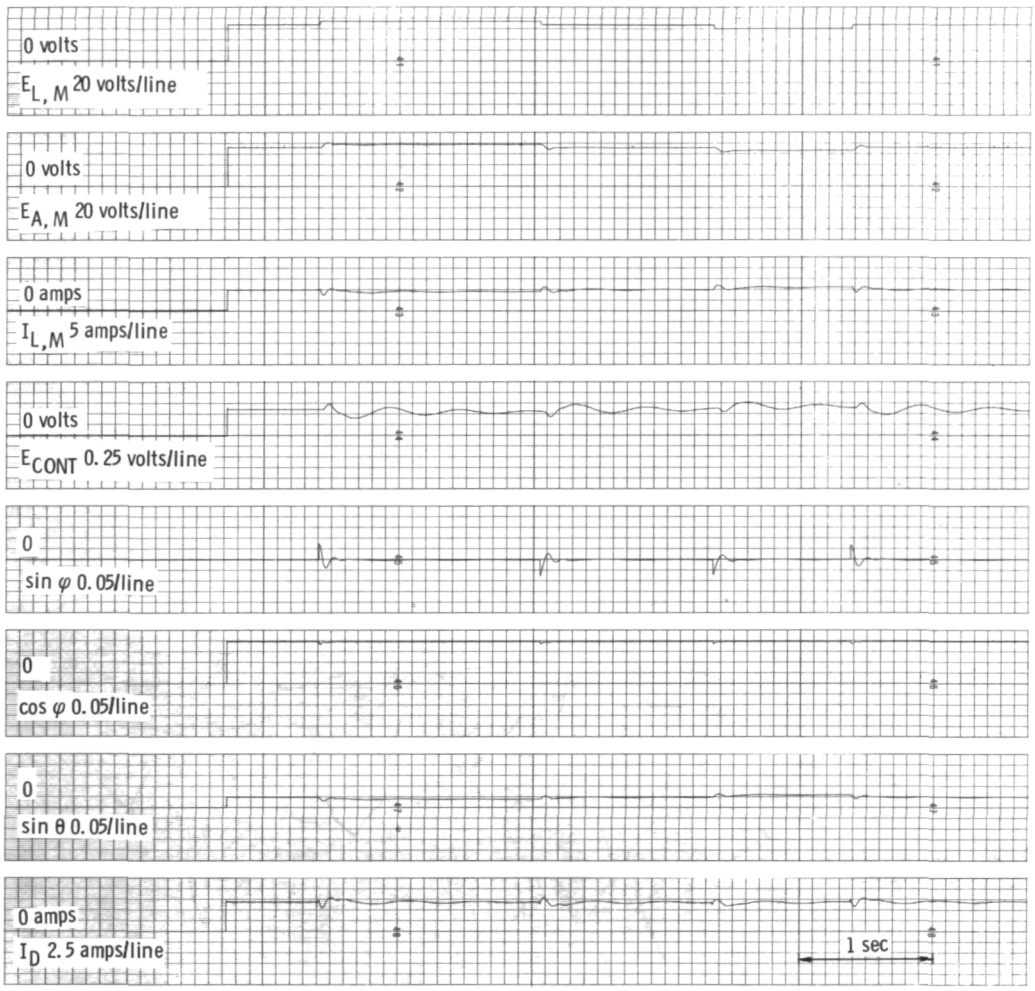

Figure 16. - ±10% step transients on $E_{L,M}$ at 100 mW/cm^2.

Figure 16. - Concluded.

Figure 17. - ±10% step transients on $E_{L,M}$ at 33 mW/cm^2.

Figure 17. - Concluded.

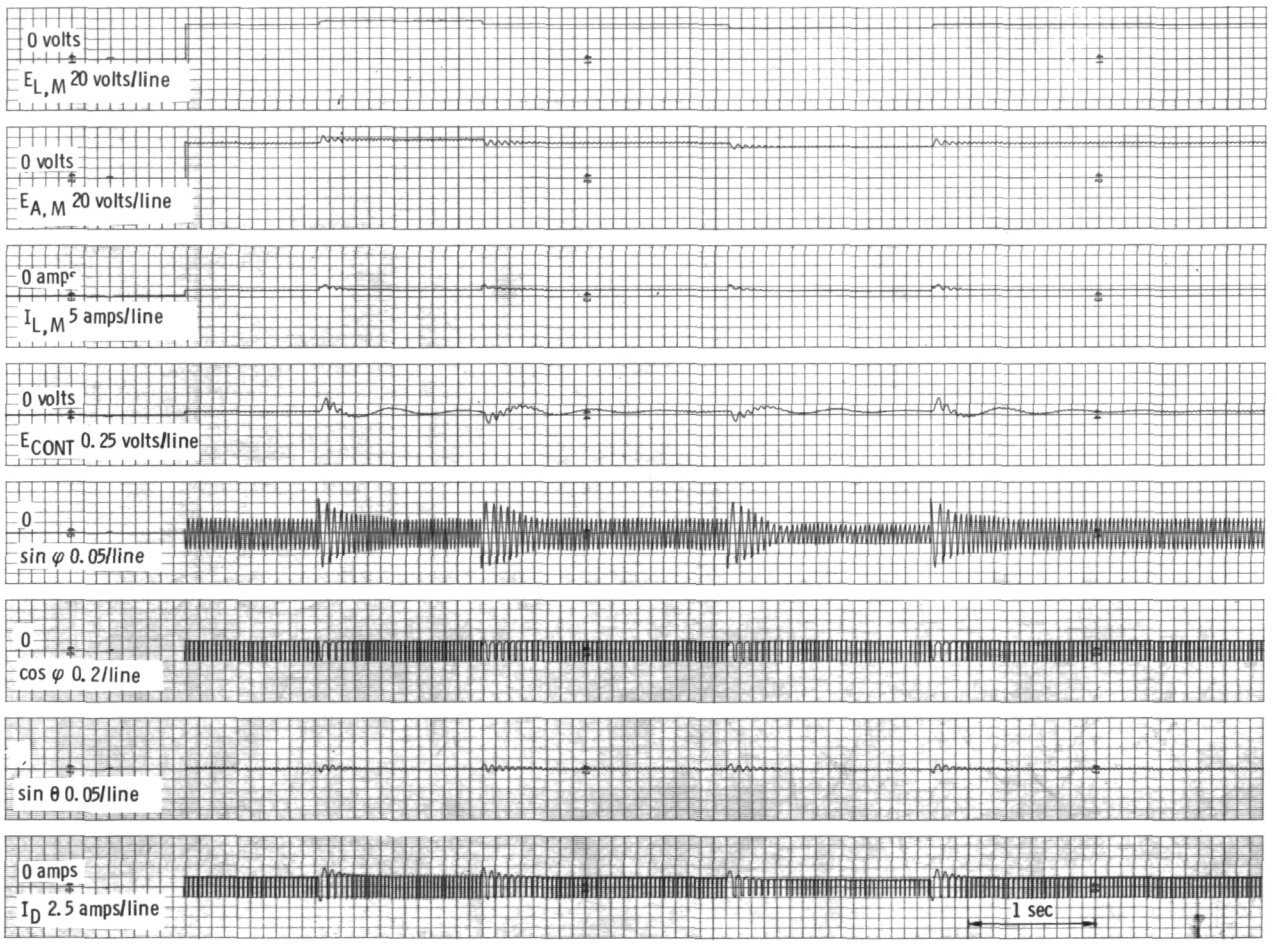

Figure 18. - ±10% step transients on $E_{L,M}$ at 14 mW/cm^2.

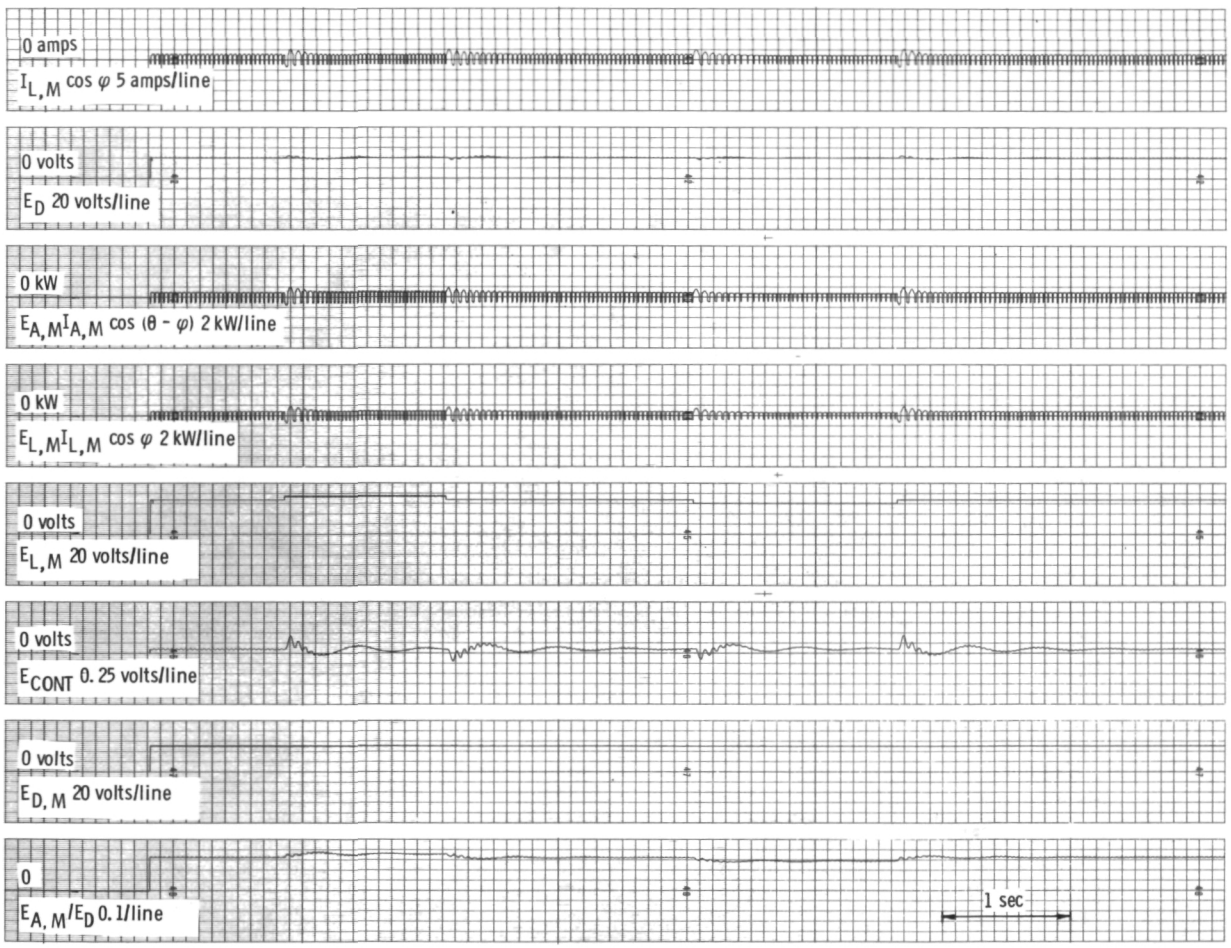

Figure 18. - Concluded.

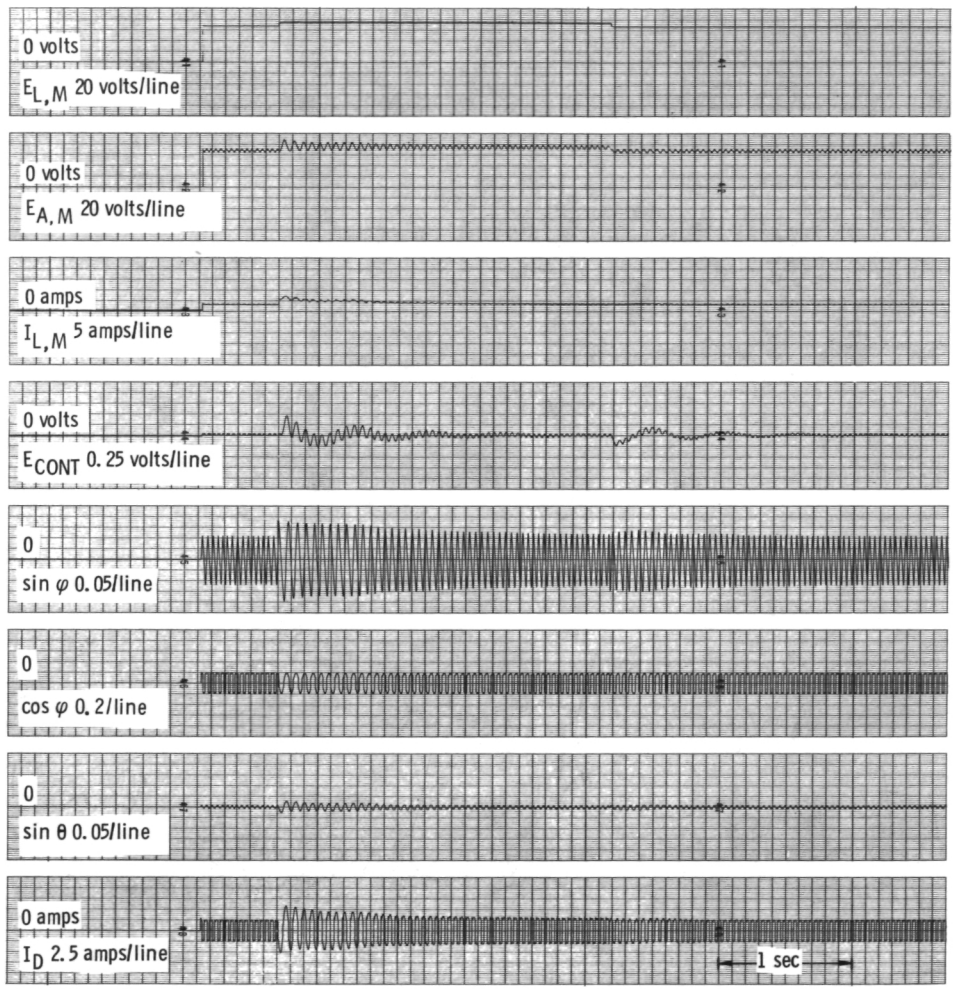

Figure 19. - ±10% step transients on $E_{L,M}$ at 6.5 mW/cm^2.

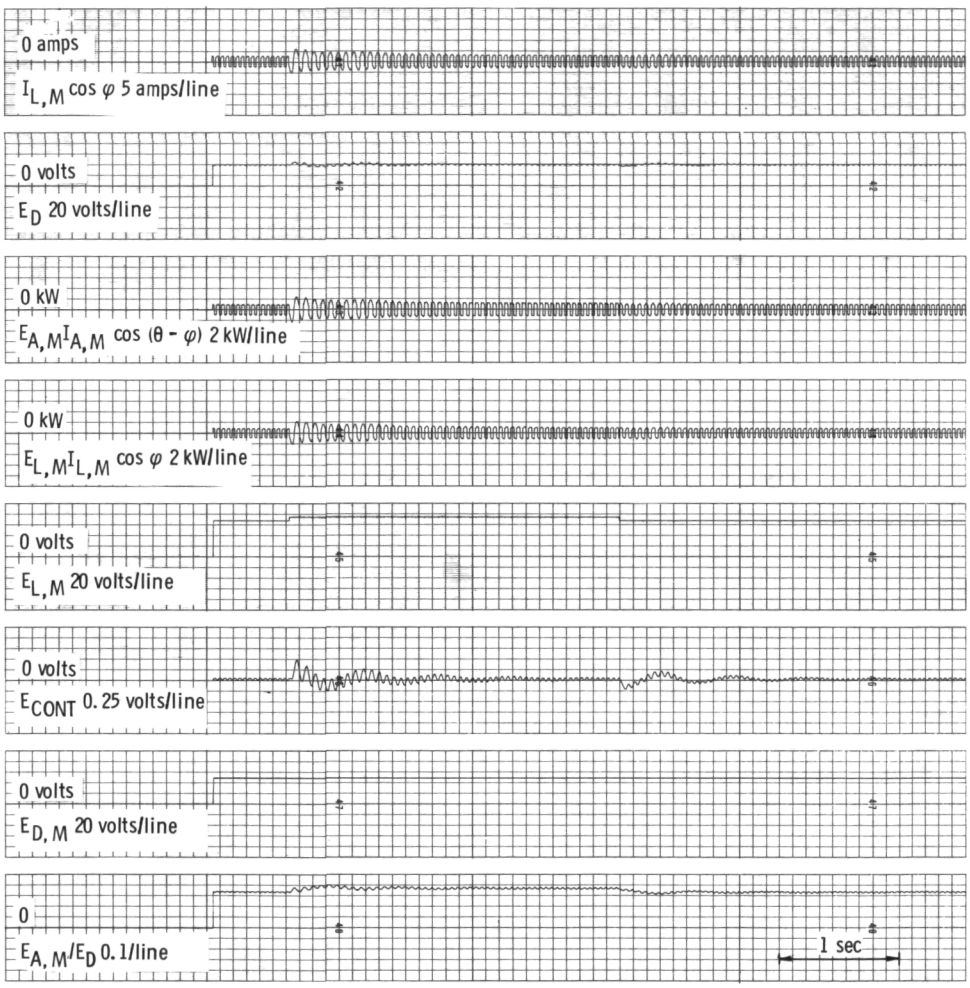

Figure 19. - Concluded.

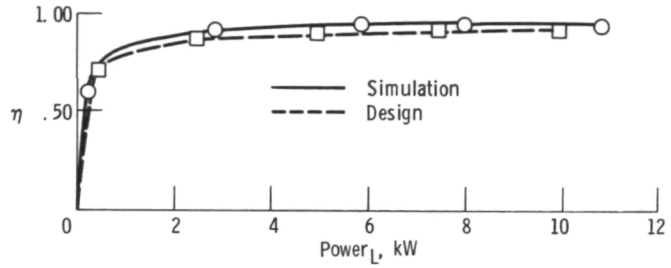

Figure 20. - Simulation and design inverter efficiencies vs. injected line power.

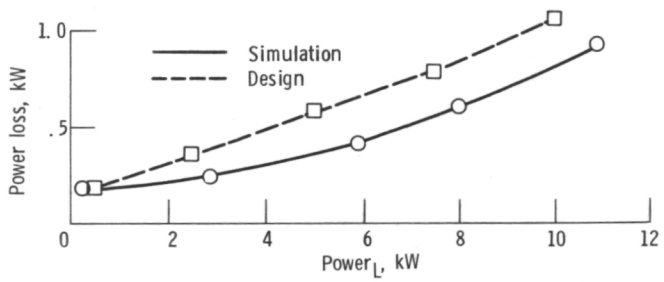

Figure 21. - Simulation and design inverter power loss vs. injected line power.

1. Report No.	2. Government Accession No.	3. Recipient's Catalog No.
NASA TM-78880		

4. Title and Subtitle	5. Report Date
PERFORMANCE AND STABILITY ANALYSIS OF A PHOTOVOLTAIC POWER SYSTEM	August 1978
	6. Performing Organization Code
7. Author(s)	8. Performing Organization Report No.
Walter C. Merrill, Ronald J. Blaha, and Roy L. Pickrell	E-9609
	10. Work Unit No.
9. Performing Organization Name and Address	
National Aeronautics and Space Administration Lewis Research Center Cleveland, Ohio 44135	11. Contract or Grant No.
	13. Type of Report and Period Covered
12. Sponsoring Agency Name and Address	Technical Memorandum
U.S. Department of Energy Division of Solar Energy Washington, D.C. 20545	14. Sponsoring Agency ~~Code~~ Report No. DOE/NASA/1022-78/30

15. Supplementary Notes

Final report. Prepared under Interagency Agreement E(49-26)-1022.

16. Abstract

Recently much emphasis has been placed on the conversion of solar energy to more useable energy forms. One method is the direct conversion of solar insolation to a dc voltage and current by the use of solar cells. This dc power can then be "inverted" to ac power compatible with commercial utility lines to drive various ac loads. This report studies the performance and stability characteristics of one such system, a 10 kVA photovoltaic power system. The system is studied using linear Bode analysis and a nonlinear analog simulation. Power conversion efficiencies, system stability, and system transient performance results are given for system operation at various levels of solar insolation. Additionally, system operation and the modeling of system components for the purpose of computer simulation are described in this report.

17. Key Words (Suggested by Author(s))	18. Distribution Statement
Photovoltaic system Dynamic simulation and modeling control Inverters Solar energy	Unclassified - unlimited STAR Category 07 DOE Category UC-63a

19. Security Classif. (of this report)	20. Security Classif. (of this page)	21. No. of Pages	22. Price*
Unclassified	Unclassified	41	A02

* For sale by the National Technical Information Service, Springfield, Virginia 22161

NASA-Langley, 1978

National Aeronautics and
Space Administration

Washington, D.C.
20546

Official Business
Penalty for Private Use, $300

SPECIAL FOURTH CLASS MAIL
BOOK

Postage and Fees Paid
National Aeronautics and
Space Administration
NASA-451

U.S.MAIL

15 2 1U,A, 072878 S90844HU
MCDONNELL DOUGLAS CORP
ATTN: PUBLICATIONS GROUP PR 15246-A
P O BOX 516
ST LOUIS MO 63166

NASA

POSTMASTER: If Undeliverable (Section 158 Postal Manual) Do Not Return